PROCEEDINGS, 48th Workshop on Geothermal Reservoir Engineering
Stanford University, Stanford, California, February 6-8, 2023
SGP-TR-224

Building the Fracture Network Model for Okuaizu Geothermal Field Based on Microseismic Data Analysis

Dian Darisma[1,2], Yusuke Mukuhira[3], Naoki Aoyogi[4], Kyosuke Okamoto[4], Takuya Ishibashi[4], Hiroshi Asanuma[4], Takatoshi Ito[3]

[1]Graduate School of Environmental Studies, Tohoku University, Sendai, Miyagi, 980-8572, Japan

[2]Department of Geophysical Engineering, Universitas Syiah Kuala, Banda Aceh, Aceh, 23111, Indonesia

[3]Institute of Fluid Science, Tohoku University, Sendai, Miyagi, 980-8577, Japan

[4]AIST-FREA, Koriyama, Fukushima, 963-0298, Japan

dian.darisma.s4@dc.tohoku.ac.jp

Keywords: microseismicity, hypocenter location, cross correlation, clustering, fracture network model

ABSTRACT

In a geothermal field, microseismicity is used to monitor subsurface conditions, especially in a geothermal reservoir. Hypocenter location can provide us with information about existing fractures as well as permeable zones. Therefore, the fracture network model based on real data sets benefits reservoir modeling. This study uses microseismic clustering analysis to build the fracture network model for Okuaizu Geothermal Field in Japan. The microseismic monitoring has been operated using nine seismic stations, consisting of five surface stations and four borehole stations. However, the previous study focused on the triggering process during injection, and the fracture system of this field has not been well understood. In this study, we analyzed microseismic data to get a more precise hypocenter location using the extended period of data during the reinjection process from 2019 to 2021. First, we located the absolute locations for 8,199 events with manually picked P- and S- wave arrival information with a homogeneous seismic velocity model. The more precise 4,235 locations were relocated using Growcust. Most of the seismic activity triggered during reinjection was concentrated at the bottom of the reinjection well. We limited the relocation results using cross correlation (CC) above 0.6 and filtered using a frequency of 5-20 Hz. Using a hierarchical clustering algorithm, Growclust, we also successfully identified some clusters in the northeast and southern parts of the injection well, which have the same trend as the NNE-SSW fault. The cluster results also correlate with microseismicity distribution by time.

1. INTRODUCTION

Microseismic monitoring has several purposes in the geothermal industry, such as reservoir characterization, production optimization, detection and mitigation of induced seismicity, and reservoir management. During water injection into geothermal reservoirs, it is essential to monitor the migration of the water to avoid cooling the reservoir and to recover steam efficiently. For this purpose, microseismic monitoring has been widely used to estimate the spatiotemporal behavior of reservoirs (Hopp et al., 2020; Kwiatek et al., 2019; Mukuhira et al., 2013). We can extract the location of the seismic event triggered during the injection process from microseismic monitoring. The hypocenter location is estimated based on information on seismic station location, travel time from the earthquake source to the stations, and velocity model. Hypocenter location can provide us with information about existing fractures. More generally, seismicity induced in geothermal fields can provide field-scale environments in which faulting and fluid flow interactions can be studied where the geology is well known (Rutledge et al., 2004). Getting a precise location is very important so we can estimate the location of permeable fractures. Therefore, relocation techniques such as the double-difference algorithm as applied to the various geothermal fields to improve the hypocenter determination such as in Tarutung-Indonesia (Muksin et al., 2014), Torre Alfina-Italy (Braun et al., 2018), Kakkonda-Japan (Okamoto et al., 2022), and Hengil-Iceland (Grigoli et al., 2022). For example, the Basel field with a 20-m error suggested that the precise locations (errors on the order of 10^1 m) can be estimated from the evolution of microseismic events (Asanuma et al., 2008).

In many such reservoirs, especially in low-porosity rocks, fracture networks can be the main pathways for the injection/extraction of these fluids (Gale et al., 2014; Vidal and Genter, 2018). However, since the fracture networks are typically located too far below direct access, such a characterization is challenging. Different approaches, including outcrop mapping have addressed it, evaluating well logs and drill cores, stochastic and geomechanical modeling (Lei et al., 2017), or, like in this study, analyzing induced seismicity. Imaging the fracture network by microseismicity analysis has the advantage that it provides 3-D information directly about the reservoir (Koepke et al., 2020).

This study will focus on Okuaizu Geothermal Field (OGF), one of Japan's largest hydrothermal geothermal fields (Figure 1). The OGF reservoir comprises a complex fracture system and is dominated by steam. Active microseismicity relates to fluid flows in the geothermal reservoir and the background tectonic faulting. Several studies have been conducted in this field to investigate the triggering process of microseismic events during injection test activity in 2015 (Okamoto et al., 2018, 2020, 2021). They found a complex structure of possible flow paths (Okamoto et al., 2018). The triggering process created a cluster in the first post-termination period of injection and in the second post-termination period was inactive due to insufficient pore-pressure migration derived from lower well bottom pressure (Okamoto et al., 2020). Previous studies have not focused on the fracture system in OGF, which makes the fracture system in this field still questionable. Therefore, this study aims to build a fracture network model using microseismic data analysis. This paper will also

elaborate on how the microseismic events are clustered to identify the fracture network using Growclust (Trugman and Shearer, 2017). The algorithm uses cross-correlation information to identify similar waveforms, and these events are then considered close to each other, most likely on the same fracture (Moriya et al., 2002). Clustering techniques can be applied to the microseismic events to understand the spatial distribution of fractures and identify any patterns or clusters that might be related to the fracture network.

2. DATA AND METHOD

2.1 Field Overview

The OGF is located 10 km west of the Aizu Basin, 10 km east of Numazawa caldera, and about 50 km behind the volcanic front of the northeast Japan arc, which is associated with the westward subduction of the Pacific Plate along the Japan Trench. Geothermal manifestations include hot springs over 90^0C, H_2S and CO_2 gas discharge, hydrothermal alteration, and abandoned sulfur and clay mines. This field is characterized by rhyolitic volcanism of about 0.3–0.2 Ma that formed Sunagohara volcano. Drill core geology indicates that volcanism began with a caldera-forming eruption in the center of this field, creating a 2-km-diameter funnel-shaped caldera. Subsequently, a fault-bounded block, including this caldera, subsided to form a 5-km-wide lake that accumulated lake sediments. Post-caldera volcanism formed lava domes and intrusions within the lake and deposited ash-flow tuffs in and around the lake. The hydrothermal system of this field is strongly controlled by sub-vertical faults that have no relation to the volcanism. The principal production zone occurs at a depth of 1.0–2.6 km within fractured Neogene formations along two NW-SE trending faults, Chinoikezawa and Sarukurazawa. These faults also formed fracture zones in the lake sediments, but there was no apparent offset of the sediments. Stratigraphic studies suggest that post-caldera activities of the Sunagohara volcano have migrated southeastward to the present high-temperature zone. The source magma of the Sunagohara volcano may contribute to the thermal potential of this field (Mizugaki, 2000). In this seismically active region, a seismic event with a magnitude of 4.9 occurred on October 12, 2009 (before the water injection test), which was concluded as a natural earthquake independent of the geothermal development. There were four seismic events with local magnitude (M_L) $\geq$ 2.7 in this region since 2016: M_L 3.6 (January 13, 2017), M_L 3.6 (January 21, 2018), M_L 2.7 (August 17, 2019), and M_L 2.8 (August 17, 2019). In addition, two seismic events with M_L 2.3 occurred on October 9, 2020, within several seconds at almost the same location. We considered these two seismic events as one seismic event with M_L 2.5. There were five seismic events with $M_L \geq 2.5$ since 2016, which seemed to occur regardless of the water injection operation (Okamoto et al., 2021).

As part of the "Technology to Evaluate and Manage Geothermal Reservoirs" project conducted by the Japan Oil, Gas and Metals National Corporation (JOGMEC) (e.g., Okabe et al. 2016), a continuous water injection (without pressurization; the average wellhead pressure during injection was 0.17 MPa) test was conducted in the Okuaizu Geothermal Field (OGF), Fukushima, Japan. The injection tests were performed from June to August 2015 to prevent the reduction in steam production. The total amount of injected fluid was approximately 1.2×10^5 m^3. During the initial stage of the test (days 0–60), the injection rate was 50 m^3/h ($1.39 \times 10{-}2$ m^3/s); in the final stage (day 60 to the end of injection), the rate was 70 m^3/h ($1.94 \times 10{-}2$ m^3/s). It took roughly ten days from the start of the injection before the injection rate was stabilized to 50 m^3/h. Figure 1 shows the injection well and the injection points, which are indicated by the green line and blue circles, respectively.

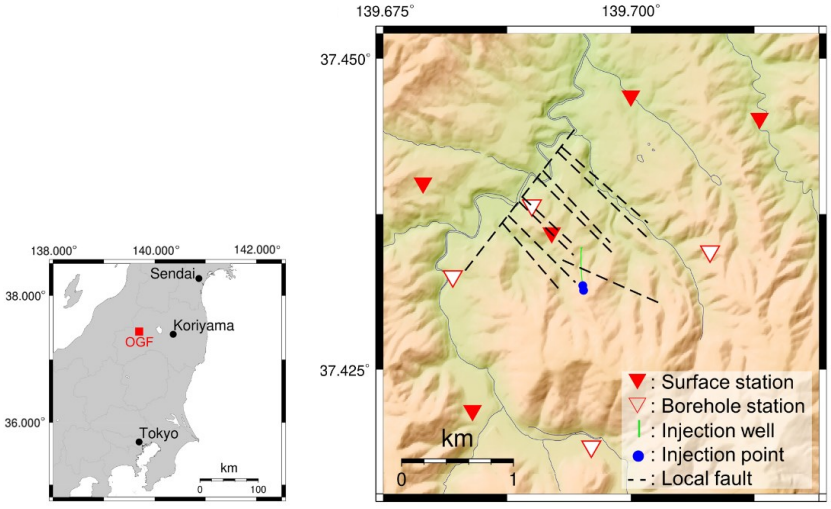

Figure 1: Map of the Okuaizu Geothermal Field (Okamoto et al., 2020).

2.2 Data

Nine seismic monitoring networks with sampling rates of 1,000 Hz, consisting of four borehole stations and five surface stations, were installed to cover the seismic activity during the fluid injection process (Figure 1). The surface and borehole sensors are Trillium Compact Posthole 20 s (Nanometrics Inc.) and F41-15.0 (International Earth Sciences IESE Ltd.), respectively, and the logger is the Centaur digital recorder (Nanometrics Inc.). Continuous seismic records are transmitted to a National Institute of Advanced Industrial Science and

Technology server in real time. Hypocenters are routinely determined by the manual selection of P-wave arrivals. At most, the residuals in P-wave travel times for the estimated hypocenters are 100 ms (~ 10^2-m error in the spatial domain). The lower limit of the detectable local seismic magnitude is approximately – 2.0 (Okamoto et al., 2018). During the injection test, roughly 1000 microseismic events were detected. The borehole stations were installed at a depth of 280-390 m, and the surface stations were buried at several meters. This study used data from 2019 to 2021. In this area, regionally, shallow soft layers (e.g., Vs < 1000 m/s) were deposited only at a depth of approximately 50 m, and the lower layer (VS ≃ 2250 m/s) extended to a depth of more than 2000 m. For simplicity, we employed a uniform velocity structure for P and S waves (Vp = 3900 m/s, Vs = 2250 m/s) following previous studies (Okamoto et al., 2018, 2020).

2.3 Method of hypocenter determination

Hypoinverse has been widely used to determine the absolute location of the earthquake (Freid, 2002). The hypocenter determination process employs a non-linear least squares algorithm to invert the hypocenter location. It also evaluates the uncertainty in hypocenter determination. In this research, the P- and S-wave arrivals were picked manually. A homogenous elastic wave velocity structure (Vp = 3900 m/s and Vp Vs = 2250 m/s) for OGF was employed for the hypocenter determination. From all the events determined by Hypoinverse, we extracted reliable seismic events based on root mean square (RMS) criteria of travel time less than 0.2 s and the hypocenter depth below 6 km. We removed all the events with "D" remarks by Hypoinverse and only used A, B, and C. Then, we relocate hypocenter locations using the hierarchical clustering algorithm (Growclust) (Trugman and Shearer, 2017). Growclust is a new alternative relocation method as part of the standard seismological analysis. The method uses input differential travel times, cross-correlation values, and reference starting locations and applies a hybrid, hierarchical clustering algorithm to simultaneously group and relocate events within similar event clusters. The cluster results can help us define any cluster related to any fracture. We used the same velocity model that applied to Hypoinverse to predict travel times and calculate differential times between earthquakes to relocate them. A maximum station distance of 5 km and a maximum RMS differential time residual of 0.2 s for cluster merger is used in the Growclust algorithm. We use cross correlation above 0.6. To be considered in later analysis, relocated earthquakes must have P- and S-phase rms residual differential less than 0.2 s, and contain five or more events in its respective Growclust branch, and five or more phase differential times used in the relocation.

2.4 Waveform similarity evaluation

We use the cross correlation method to provide a better travel time difference as input data to Growclust (Deichmann and Garcia-Fernandez, 1992). Cross correlation can remove the potential bias from human detection in the catalog pick and provide more objective and precise travel time difference detection, which leads to better hypocenter location. The similarity of the two waveforms is evaluated with cross correlation, and their lag time between two events is used as differential time. The similarity of the waveforms is checked for all possible pairs of events on the same station and component. Kwiatek et al. (2014) find that the best average precision of hypocenters is obtained for a range of the cross-correlation coefficient between 0.6 and 0.75. However, selecting the highest possible threshold (0.75) significantly reduces the number of data used (Bulut et al., 2011). Waldhauser and Schaff (2008) concluded that a cross-correlation coefficient of 0.7 was a threshold to avoid substantial outliers based on the Northern California Seismic Network data. They used a 1 s time window and a 1.5–15 Hz band-pass filter. In this study, we corrected P- and S-wave arrival with cross correlation in 5-20 Hz, as shown in Figure 2, with a time window of 0.05 s before P- and S-wave, and 0.2 s and 0.3 after P- and S-wave, respectively. We calculate all the cross-correlation pairs based on absolute location waveform information for all the stations. We use the vertical component to correct P-wave and the horizontal component for S-wave.

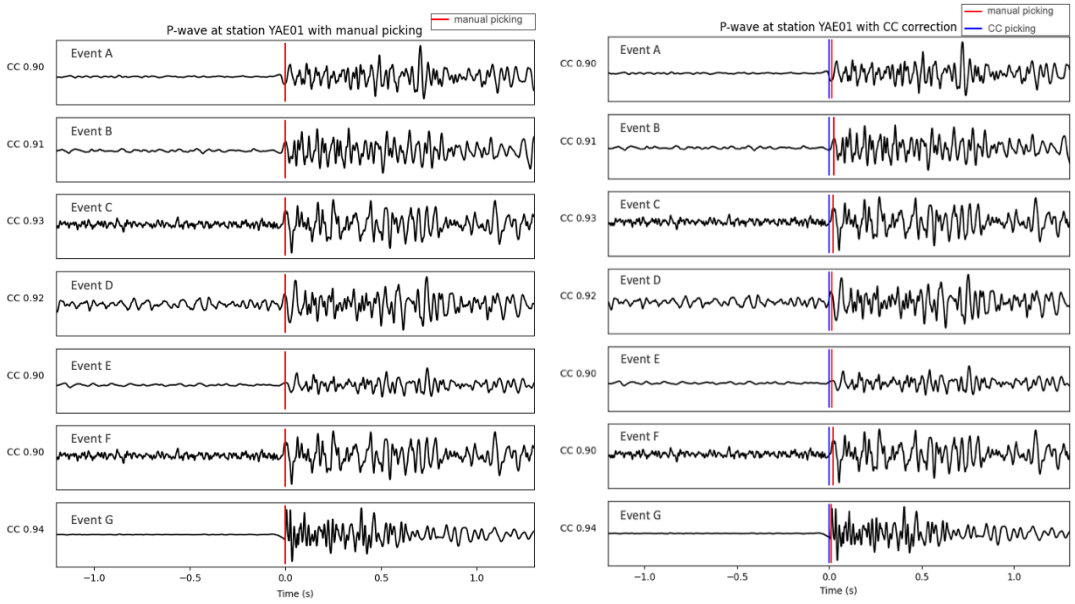

Figure 2: Examples of waveforms around P-wave arrival recorded YAE06. The Left shows the manual pick results, and the right shows the comparison with cross correlation corrected pick results

3. RESULTS AND DISCUSSION

We successfully located 8,199 absolute locations using data from January 2019 to September 2021 (Table 1) and removed bad events with a "D" remark by Hypoinverse and located above 6 km. All the locations have RMS errors below 0.2 s, corresponding to spatial errors around 200 m. We plot all the events to see how they change over time (Figure 3). The biggest seismicity recorded was in the middle of November 2020, with almost reaching 180 events in a day. On average, we recorded about 20-40 events per day. Most microseismic events are concentrated near the bottom well (Figure 5-7). However, some events are in the unreasonably shallow part, which could be an artifact. Entire microseismic events show a very cloud-like distribution, and no apparent seismic structure is presented.

Table 1: Information about total events located by Hypoinverse and Growclust, the parameter of cross-correlation event pair, and median horizontal error (EH) and vertical error (EV) by Growclust

Year	Hypoinverse	Event pairs	CC event pairs	Growclust	Median EH	Median EV
2019	2,929	75,285	567,480	1,353	36 m	23 m
2020	2,880	313,640	2,438,831	1,386	38 m	22 m
2021	2,390	181,202	1,372,229	1,496	42 m	28 m
Total	8,199	570,127	4,378,540	4,235		

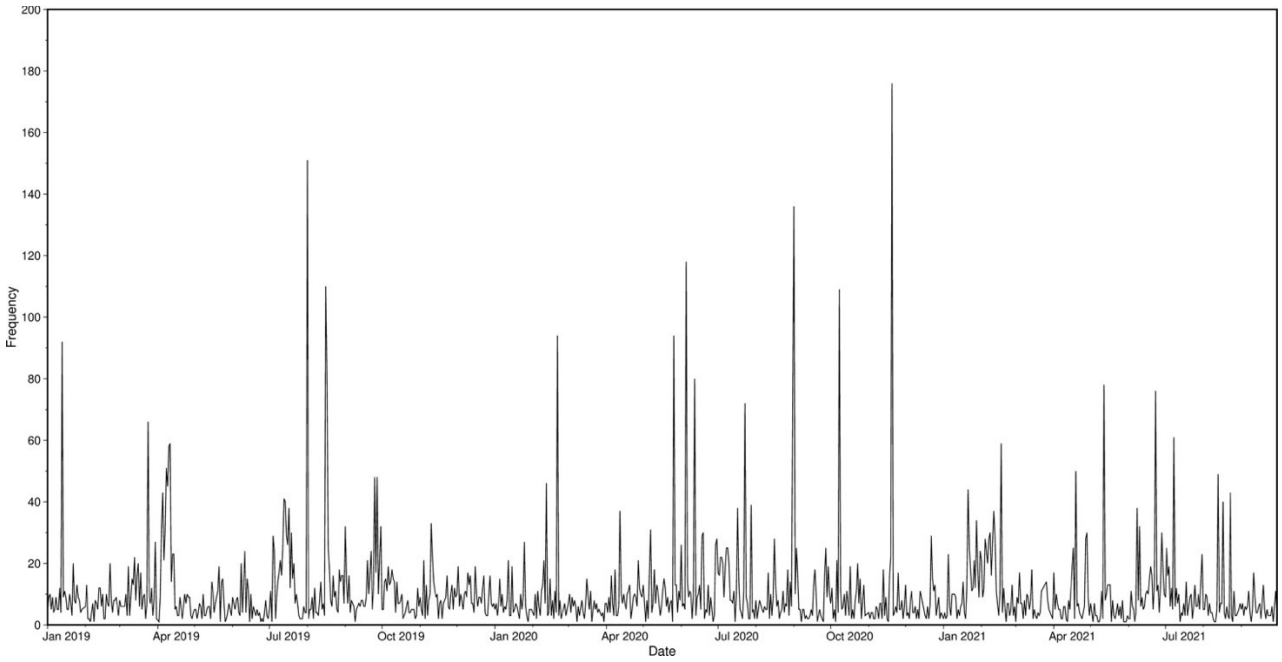

Figure 3: Frequency of microseismic events detected for each day from 2019 until 2021.

Figure 4 shows the cross-correlation result at station YAE06 and the ratio of cross-correlation calculation. The results show that cross-correlation results at this station have a cross correlation value above 0.6, around 48%, and only 1% cross-correlation value above 0.9. This ratio correlates with the complexity of the reservoir structures. Before we relocate the absolute location using Growclust, we try using HypoDD, but the code cannot handle a big cross-correlation data. We relocate the event hypocenters using Growclust for 4,235 events, or about 52% of absolute locations, using 4,378,540 cross-correlation event pairs (Table 1). The seismic cloud gets tight in general. With these improvements, the RMS error was also improved below 0.01 s with a mean spatial error around 36 m and 23 m for horizontal and vertical 2019 events, respectively. The 2020 and 2021 results also give almost the same error number. The seismic distribution is also not as scattered as the Hypoinverse results. If we compare the CC pairs for each year, the number for 2019 is the smallest, with 567,480 event pairs. Data from 2019 have 51 clusters, the biggest cluster, followed by data in 2020 with 45 clusters and data in 2021 with 32 clusters. The cluster number is two times smaller if we set the events number for each branch for ten events. This can be why some events trigger minor fractures with less than ten events.

We found that the relocation results for 2019 (Figure 5) and 2021 (Figure 7) almost have the same pattern: the big cluster focuses on the northern part of the injection well. But for the 2020 results, the seismic events decreased in this area and increased in the southern part of

the injection well (Figure 6). Seismic distribution in the injection well's northeast part is considered an existing fault with direction NNW-SSE (New Energy Development Organization, 1997). Okamoto et al. (2020) also found two significant clusters using 3-month data during an injection test in 2015 and compared it with tomography results. They suggested that the area has higher velocities than the surrounding area, and between those two clusters identified as a highly permeable fracture. The cluster results also significantly correlate with microseismicity distribution by time (Figure 8). For example, a cluster from 2020 events in the northeast part of the injection well (shown by the green color in Figure 6). The big cluster during that period triggered around October and November (Figure 3) and has the same fault trend as the NNW-SSE fault in the area. Figure 8 also confirms that the microseismic distribution in the OGF has two significant clusters located in the northeast part and southern parts of the injection well.

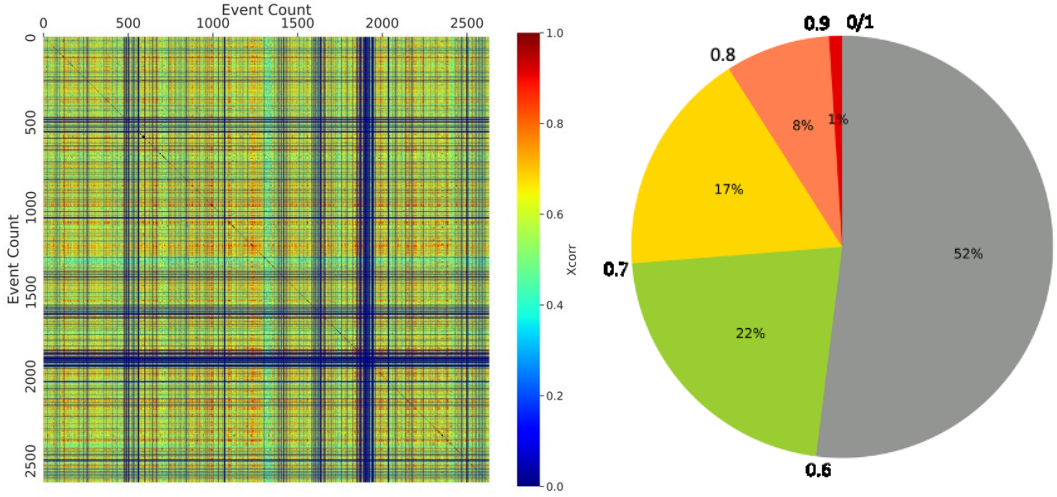

Figure 4: Cross-correlation matrix at station YAE06 2021 (left) and the ratio of cross correlation from station YAE06 (right).

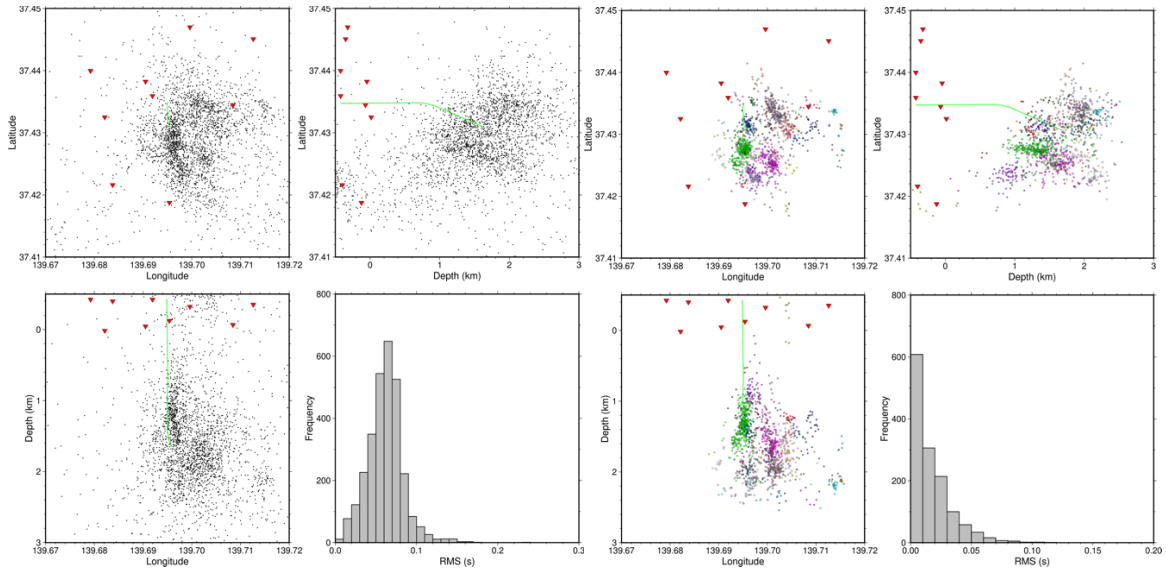

Figure 5: Absolute location of microseismicity in 2019 located using Hypoinverse (left). The red triangles are seismic stations, and the green line is an injection well. Right: Hypocenter distribution relocated using Growclust for 2019 data. Different colors show different clusters. The green color is the big cluster with 314 events.

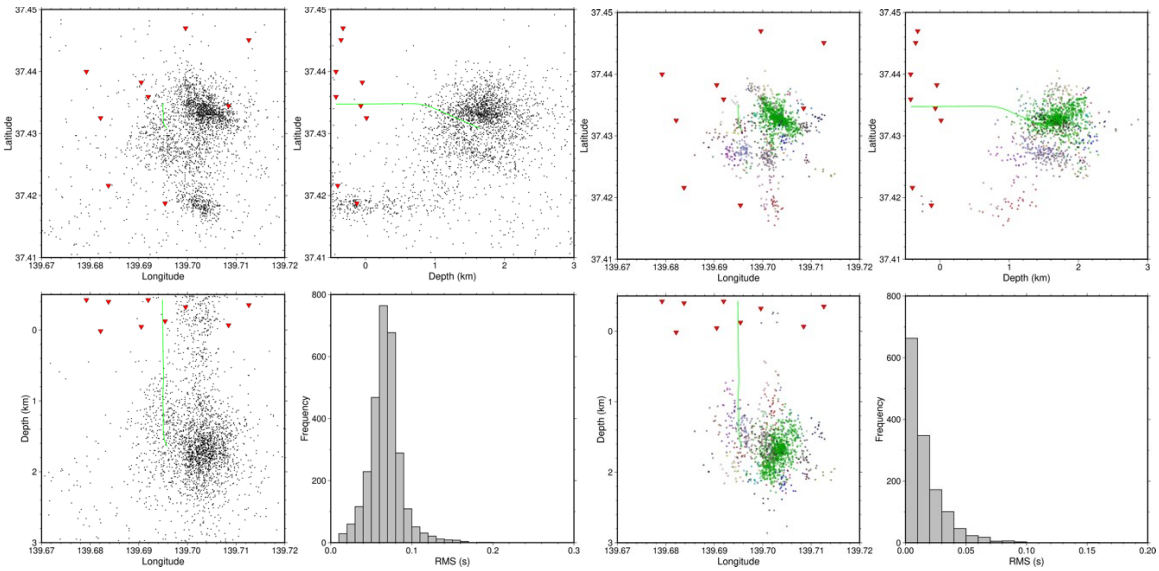

Figure 6: Absolute location of microseismicity in 2020 located using Hypoinverse (left). The red triangles are seismic stations, and the green line is an injection well. Right: Hypocenter distribution relocated using Growclust for 2020 data. Different colors show different clusters. The green color is the big cluster for 840 events.

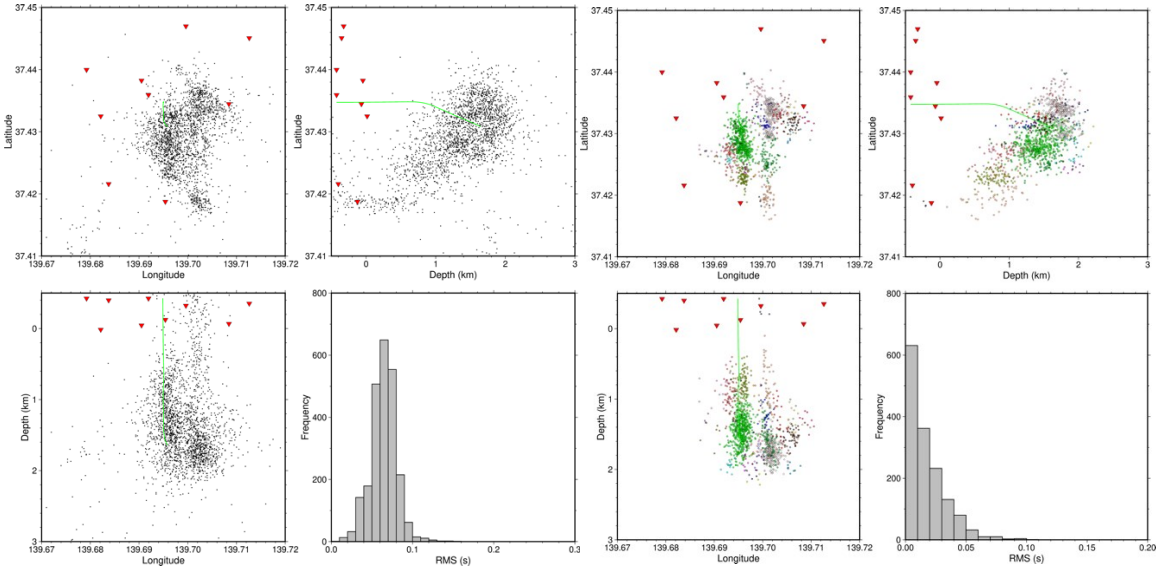

Figure 7: Absolute location of microseismicity in 2021 located using Hypoinverse (left). The red triangles are seismic stations, and the green line is an injection well. Right: Hypocenter distribution relocated using Growclust for 2021 data. Different colors show different clusters. The green color is the big cluster with 520 events.

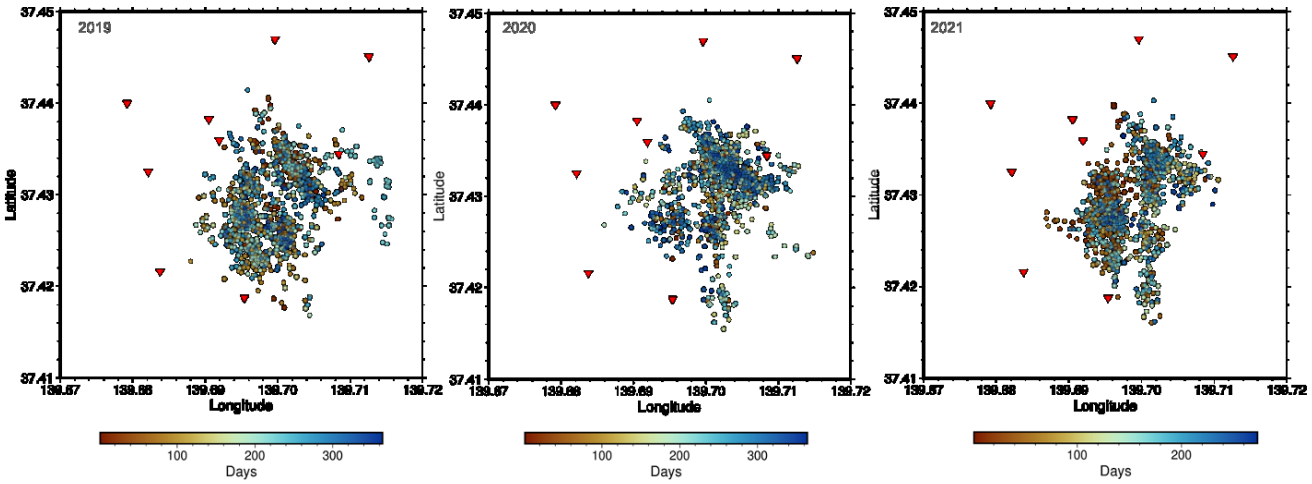

Figure 8: Microseismic distribution by time from the top view of 2019 (left), 2020 (middle), and 2021 (right).

5. CONCLUSION

In this paper, we located three years of data on seismic events from 2019 to 2021 using nine stations, consisting of four borehole stations and five surface stations. To get a precise location, we successfully relocated 52% of absolute locations using Growclust. To be considered in later analysis, we use cross correlation above 0.6; relocated earthquake must have P- and S-phase rms residual differential less than 0.2 s and contain five or more events in its respective Growclust branch and five or more phase differential times used in the relocation. The relocation results show two big clusters in the northeast part of the injection well and the southern part of the injection well. Some of the big cluster show structure in the direction of NNW-SSE. The cluster results also show a big correlation with microseismicity distribution by time.

ACKNOWLEDGMENT

This study was performed as a part of the "Technology to evaluate and manage geothermal reservoirs" sponsored by Japan Organization for Metals and Energy Security (JOGMEC).

REFERENCES

Asanuma, H., Kumano, Y., Niitsuma, H., Schanz, U., Häring, M.: Interpretation of Reservoir Structure from Super-Resolution Mapping of Microseismic Multiplets from Stimulation at Basel, Switzerland in 2006. GRC Transactions 32, (2008), 53–58.

Bulut, F., Ellsworth, W.L., Bohnhoff, M., Aktar, M., Dresen, G.: Spatiotemporal Earthquake Clusters along the North Anatolian Fault Zone Offshore İstanbul. Bulletin of the Seismological Society of America 101, (2011), 1759–1768. https://doi.org/10.1785/0120100215

Deichmann, N., Garcia-Fernandez, M.: Rupture geometry from high-precision relative hypocentre locations of microearthquake clusters. Geophysical Journal International 110, (1992), 501–517. https://doi.org/10.1111/j.1365-246X.1992.tb02088.x

Freid, K.: User's Guide to HYPOINVERSE-2000, a Fortran Program to Solve for Earthquake Locations and Magnitudes (Open-File Report), Open-File Report. Menlo Park CA, (2002).

Gale, J.F.W., Laubach, S.E., Olson, J.E., Eichhuble, P., Fall, A.: Natural Fractures in shale: A review and new observations. Bulletin 98, (2014), 2165–2216. https://doi.org/10.1306/08121413151

Hopp, C., Sewell, S., Mroczek, S., Savage, M., Townend, J.: Seismic response to evolving injection at the Rotokawa geothermal field, New Zealand. Geothermics 85, (2020), 101750. https://doi.org/10.1016/j.geothermics.2019.101750

Koepke, R., Gaucher, E., Kohl, T.: Pseudo-probabilistic identification of fracture network in seismic clouds driven by source parameters. Geophysical Journal International 223, (2020), 2066–2084. https://doi.org/10.1093/gji/ggaa441

Kwiatek, G., Bulut, F., Bohnhoff, M., Dresen, G. High-resolution analysis of seismicity induced at Berlín geothermal field, El Salvador. Geothermics 52, (2014), 98–111. https://doi.org/10.1016/j.geothermics.2013.09.008

Kwiatek, G., Saarno, T., Ader, T., Bluemle, F., Bohnhoff, M., Chendorain, M., Dresen, G., Heikkinen, P., Kukkonen, I., Leary, P., Leonhardt, M., Malin, P., Martínez-Garzón, P., Passmore, K., Passmore, P., Valenzuela, S., Wollin, C.: Controlling fluid-induced seismicity during a 6.1-km-deep geothermal stimulation in Finland. Sci. Adv. 5, (2019), eaav7224. https://doi.org/10.1126/sciadv.aav7224

Lei, Q., Latham, J.-P., Tsang, C.-F.: The use of discrete fracture networks for modeling coupled geomechanical and hydrological behaviour of fractured rocks. Computers and Geotechnics 85, (2017), 151–176. https://doi.org/10.1016/j.compgeo.2016.12.024

Mizugaki, K., 2000. Geologic structure and volcanic history of the Yanaizu-Nishiyama (Okuaizu) geothermal field, Northeast Japan. Geothermics 29, (2000), 233-256.

Moriya, H., Nakazato, K., Niitsuma, H., Baria, R. Detailed Fracture System of the Soultz-sous-Forêts HDR Field Evaluated Using Microseismic Multiplet Analysis. pure and applied geophysics 159, (2002), 517–541. https://doi.org/10.1007/PL00001263

Mukuhira, Y., Asanuma, H., Niitsuma, H., Häring, M.O.: Characteristics of large-magnitude microseismic events recorded during and after stimulation of a geothermal reservoir at Basel, Switzerland. Geothermics 45, (2013), 1–17. https://doi.org/10.1016/j.geothermics.2012.07.005

Okamoto, K., Asanuma, H., Nimiya, H.: Fluid activity detection in geothermal areas using a single seismic station by monitoring horizontal-to-vertical spectral ratios. Sci Rep 11, (2021), 8372. https://doi.org/10.1038/s41598-021-86775-1

Okamoto, K., Yi, L., Asanuma, H., Okabe, T., Abe, Y., Tsuzuki, M.: Activation and Inactivation of Seismicity: The Terminations of Two Injection Tests in Okuaizu Geothermal Field, Japan. Seismological Research Letters 91, (2020), 2730–2743. https://doi.org/10.1785/0220200084

Okamoto, K., Yi, L., Asanuma, H., Okabe, T., Abe, Y., Tsuzuki, M.: Triggering processes of microseismic events associated with water injection in Okuaizu Geothermal Field, Japan. Earth Planets Space 70, (2018), 15. https://doi.org/10.1186/s40623-018-0787-7

Rutledge, J.T., Phillips, W.S., Mayerhofer, M.J.: Faulting Induced by Forced Fluid Injection and Fluid Flow Forced by Faulting: An Interpretation of Hydraulic-Fracture Microseismicity, Carthage Cotton Valley Gas Field, Texas. Bulletin of the Seismological Society of America 94, (2004), 1817–1830. https://doi.org/10.1785/012003257

Trugman, D.T., Shearer, P.M.: GrowClust: A Hierarchical Clustering Algorithm for Relative Earthquake Relocation, with Application to the Spanish Springs and Sheldon, Nevada, Earthquake Sequences. Seismological Research Letters 88, (2017), 379–391. https://doi.org/10.1785/0220160188

Vidal, J., Genter, A.: Overview of naturally permeable fractured reservoirs in the central and southern Upper Rhine Graben: Insights from geothermal wells. Geothermics 74, (2018), 57–73. https://doi.org/10.1016/j.geothermics.2018.02.003

Waldhauser, F., Schaff, D.P.: Large-scale relocation of two decades of Northern California seismicity using cross-correlation and double-difference methods. Journal of Geophysical Research: Solid Earth 113, (2008). https://doi.org/10.1029/2007JB005479